

**SCHOOL OF MATERIALS AND MINERAL RESOURCES ENGINEERING**  
**UNIVERSITI SAINS MALAYSIA**

**SYNTHESIS AND CHARACTERIZATION OF MANGANESE DIOXIDE  
NANOPARTICLES VIA DIRECT HEATING METHOD**

By

**WONG CHEE LEONG**

**Supervisor: Assoc. Prof. Ir. Dr. Pung Swee Yong**

Dissertation submitted in fulfillment

of the requirements for the degree of Bachelor of Engineering with Honours

(Materials Engineering)

Universiti Sains Malaysia

**JUNE 2018**

## DECLARATION

I hereby declare that I have conducted, completed the research work and written the dissertation entitled **“Synthesis and Characterization of Manganese Dioxide Nanoparticles via Direct Heating Method”**. I also declare that it has not been previously submitted for the award for any degree or diploma or other similar title of this for any other examining body or University.

Name of Student : WONG CHEE LEONG

Signature:

Date : 14 June 2018

Witnessed by

Supervisor : Assoc. Prof. Ir. Dr. Pung Swee Yong

Signature:

Date : 14 June 2018

## **ACKNOWLEDGEMENTS**

Here I would like to express my deepest sense of gratitude to those people who had helped me along this project. This project would not have been completed without them. First and foremost, I would like to express my heartfelt appreciation and thanks to my supervisor, Assoc. Prof. Ir. Dr. Pung Swee Yong for his patience guidance, advice and encouragement throughout this project. He is always be there to give me endless support whenever I faced experimental problems.

I am grateful to School of Materials and Mineral Resources Engineering, Universiti Sains Malaysia (USM) for rendering necessary environment and equipment for me to carry out my project. Millions of thanks go to technician, academic and administrative staffs for their assistance and guidance in equipment and machine handling.

In addition, special thanks to Dr Pung's research team for providing the necessary help as well as the valuable advice on the experimental work. This work would be more difficult without them.

# TABLE OF CONTENTS

<b>Contents</b>	<b>Page</b>
DECLARATION .....	ii
ACKNOWLEDGEMENTS .....	iii
TABLE OF CONTENTS .....	iv
LIST OF TABLES .....	viii
LIST OF FIGURES .....	ix
LIST OF ABBREVIATIONS .....	xiv
LIST OF SYMBOLS .....	xv
ABSTRAK .....	xvi
ABSTRACT .....	xviii
<b>CHAPTER 1</b> .....	<b>1</b>
<b>INTRODUCTION</b> .....	<b>1</b>
1.1 Research background .....	1
1.2 Problem statement .....	5
1.3 Research objectives .....	6
1.4 Project overview .....	6
1.5 Thesis outline .....	7
<b>CHAPTER 2</b> .....	<b>8</b>
<b>LITERATURE REVIEW</b> .....	<b>8</b>
2.1 Introduction .....	8

2.2 Dyes and their classification .....	8
2.3 Major sources of organic dye pollutants and their effects to human and environment.....	9
2.4 Conventional methods of organic dye removal .....	11
2.4.1 Adsorption .....	11
2.4.2 Membrane filtration.....	12
2.4.3 Ion exchange.....	13
2.4.4 Coagulation-flocculation .....	14
2.4.5 Aerobic / anaerobic degradation.....	15
2.4.6 AOPs.....	15
2.5 Manganese (Mn) and MnO <sub>x</sub> .....	22
2.6 Synthesis methods of MnO <sub>x</sub> nanomaterials .....	26
2.6.1 Physical methods .....	26
2.6.2 Chemical methods .....	28
2.6.3 Green or biological methods .....	33
2.6.4 Direct heating method .....	42
2.7 Applications of MnO <sub>x</sub> .....	42
<b>CHAPTER 3.....</b>	<b>43</b>
<b>METHODOLOGY .....</b>	<b>43</b>
3.1 Introduction.....	43
3.2 Chemical raw materials.....	44
3.3 Experimental procedures.....	45

3.3.1 Synthesis of MnO <sub>2</sub> nanoparticle using co-precipitation method .....	45
3.3.2 Synthesis of MnO <sub>2</sub> nanoparticles using sol gel method .....	46
3.3.3 Synthesis of MnO <sub>2</sub> nanoparticles using direct heating method .....	47
3.4 Characterisation techniques .....	49
3.4.1 XRD.....	50
3.4.2 XPS.....	50
3.4.3 FESEM .....	51
3.4.4 TEM/ HRTEM.....	52
3.4.5 Zetasizer .....	52
3.4.6 FTIR .....	53
3.4.7 UV-VIS.....	53
3.5 RhB dye removal study using MnO <sub>2</sub> nanoparticles .....	54
3.5.1 RhB dye removal test .....	54
3.5.2 Scavenger test.....	55
3.5.3 Repeatability test .....	55
<b>CHAPTER 4.....</b>	<b>57</b>
<b>RESULTS AND DISCUSSION .....</b>	<b>57</b>
4.1 Introduction .....	57
4.2 Synthesis and characterization of MnO <sub>2</sub> nanoparticles synthesized through co-precipitation method.....	57
4.2.1 Washing effect on MnO <sub>2</sub> nanoparticles.....	57
4.2.2 RhB dye removal study of MnO <sub>2</sub> nanoparticles.....	62

4.3 Synthesis and characterization of MnO <sub>2</sub> nanoparticles synthesized through sol gel method.....	68
4.3.1 Washing effect on MnO <sub>2</sub> nanoparticles.....	68
4.3.2 RhB dye removal study of MnO <sub>2</sub> nanoparticles.....	73
4.4 Removal mechanism of RhB dye.....	77
4.4.1 Identification of dominant active species in RhB removal process .....	77
4.4.2 Identification of adsorption behaviour of MnO <sub>2</sub> nanoparticles.....	78
4.4.3 Identification of H <sup>+</sup> in RhB removal process .....	81
4.4.4 Postulated mechanism of RhB removal process .....	82
4.5 Synthesis and characterization of MnO <sub>2</sub> nanoparticles synthesized through direct heating method .....	84
4.5.1 Effect of applied power .....	84
4.5.2 Effect of growth time.....	89
4.5.3 RhB dye removal study of MnO <sub>2</sub> nanoparticles.....	92
<b>CHAPTER 5 .....</b>	<b>95</b>
<b>CONCLUSION AND RECOMMENDATION .....</b>	<b>95</b>
5.1 Conclusion.....	95
5.2 Recommendation.....	97
<b>REFERENCES.....</b>	<b>98</b>
<b>APPENDIX.....</b>	<b>119</b>

## LIST OF TABLES

Table 2.1: Classification of dyes based on chemical structure. ....	8
Table 2.2: Common AOPs and reactions involved in each process. ....	16
Table 2.3: Advantages and disadvantages of different dye removal methods.....	19
Table 2.4: Summary of utilisation of manganese oxide on different dye removal.....	23
Table 2.5: Summary of crystallographic data and properties of some MnO <sub>2</sub> polymorphs .....	25
Table 2.6: Advantages and disadvantages of different synthesis methods.....	39
Table 3.1: Chemical and materials used during this project.....	44
Table 3.2: Parameter studied in MnO <sub>2</sub> nanoparticles synthesis via co-precipitation method.....	45
Table 3.3: Parameter studied in MnO <sub>2</sub> nanoparticles synthesis via sol gel method.....	46
Table 3.4: Summary of the parameters studied in direct heating synthesis.....	48
Table 3.5: Scavenger involved in removal test.....	55
Table 4.1: Comparison of RhB removal efficiency with the work reported in literature.....	76
Table 4.2: Checklist of the indicator for photocatalytic degradation, adsorption and oxidative degradation. ....	82



## LIST OF FIGURES

Figure 1.1: River water quality trend in Malaysia from year 2010 to year 2015. ....	2
Figure 1.2: Distribution of wastewater release from textile industry in Malaysia.....	3
Figure 2.1: Export demand of textiles and textile products in Malaysia from 2010 to 2017 (in billion).....	10
Figure 2.2: Principle of surface filtration using membrane or filter cloth.....	13
Figure 2.3: Schematic diagram of ion exchange process with generalised cation- exchanger bead which bearing fixed negative charges.....	14
Figure 2.4: Coagulation and flocculation processed of a colloidal suspension.....	15
Figure 2.5: Schematic diagram of RhB degradation mechanism . ....	17
Figure 2.6: Schematic representation of different MnO <sub>2</sub> polymorphs.....	25
Figure 2.7: Schematic diagram of a thermal evaporation system.....	27
Figure 2.8: Schematic diagram of a typical sputtering deposition system .....	28
Figure 2.9: Synthesis nanoparticles using co-precipitation method .....	30
Figure 2.10: Various steps in the sol-gel process to control the final morphology of the product.....	31
Figure 2.11: Schematic representation of hydrothermal and solvothermal synthesis. ...	32
Figure 2.12: Schematic representation of reverse micelles synthesis of inorganic nanoparticles.....	33
Figure 2.13: Plant-mediated synthesis mechanism.....	35
Figure 2.14: Illustration of fungal biosynthesis. (a) Extracellular synthesis; (b) Intracellular synthesis .....	36
Figure 2.15: Summary of biometal interaction in microbial system .....	38

Figure 3.1: Project summary.....	43
Figure 3.2: Schematic flow diagram of MnO <sub>2</sub> nanoparticles synthesis by co-precipitation method.....	46
Figure 3.3: Schematic flow diagram of MnO <sub>2</sub> nanoparticles by sol gel method.....	47
Figure 3.4: Winding wire around the middle of mechanical pencil. ....	47
Figure 3.5: Cleaned wire coil for MnO <sub>2</sub> nanoparticles synthesis via direct heating method.....	48
Figure 3.6: Experimental setup for growth of MnO <sub>2</sub> nanoparticles on wire coil via direct heating synthesis. ....	49
Figure 4.1: XRD patterns of washed and unwashed co-precipitated MnO <sub>2</sub> nanoparticles.....	58
Figure 4.2: XPS spectra of the MnO <sub>2</sub> nanoparticles synthesized by co-precipitation method, (a) survey scan; (b) K 2p spectrum; (c) Mn 2p spectrum; (d) O 1s spectrum. ....	59
Figure 4.3: SEM images of (a) washed, (b) unwashed powders synthesized by co-precipitation approach.....	60
Figure 4.4: (a) TEM and (b) HRTEM images of unwashed MnO <sub>2</sub> nanoparticles synthesized by co-precipitation method.....	61
Figure 4.5: Surface zeta potential of (a) washed, (b) unwashed powders synthesized by co-precipitation approach.....	62
Figure 4.6: UV-Vis absorbance spectra of RhB solution after removal testing (a) with only HCl and (b) with only H <sub>2</sub> SO <sub>4</sub> under UV irradiation. No MnO <sub>2</sub> nanoparticles for both case.....	63
Figure 4.7: UV-Vis absorbance spectra of RhB solution after removal testing, with washed MnO <sub>2</sub> nanoparticles (a) without acid, (b) and HCl (c) and H <sub>2</sub> SO <sub>4</sub> ;	

with unwashed MnO <sub>2</sub> nanoparticles (d) without acid, (e) and HCl (f) and H <sub>2</sub> SO <sub>4</sub> under UV irradiation (co-precipitation).....	64
Figure 4.8: Colour change after degradation of RhB solution by co-precipitated MnO <sub>2</sub> at 0min, 2min, 4min, 6min, 8min, 10min and 12min with addition of (a) HCl; (b) H <sub>2</sub> SO <sub>4</sub> . ....	65
Figure 4.9: Blue shift of maximum absorbance of degraded RhB by co-precipitated MnO <sub>2</sub> nanoparticles under UV irradiation. ....	66
Figure 4.10: Removal efficiency (a) as a function of time and (b) at 12 min under UV irradiation (co-precipitation).....	67
Figure 4.11: XRD patterns of washed and unwashed MnO <sub>2</sub> nanoparticles synthesized using sol gel approach. ....	68
Figure 4.12: XPS spectra of the MnO <sub>2</sub> nanoparticles synthesized by sol gel method, (a) survey scan; (b) K 2p spectrum; (c) S 2p spectrum; (d) Mn 2p spectrum; (e) O 1s spectrum.....	70
Figure 4.13: SEM images of (a) washed and (b) unwashed MnO <sub>2</sub> nanoparticles synthesized by sol gel approach. ....	71
Figure 4.14: (a) TEM and (b) HRTEM images of unwashed MnO <sub>2</sub> nanoparticles synthesized by sol gel method. ....	72
Figure 4.15: Surface zeta potential of (a) washed, (b) unwashed powders synthesized by sol gel approach. ....	73
Figure 4.16: Colour change after degradation of RhB solution by MnO <sub>2</sub> nanoparticles synthesized by sol gel method at 0min, 2min, 4min, 6min, 8min, 10min and 12min with addition of (a) HCl; (b) H <sub>2</sub> SO <sub>4</sub> . ....	74
Figure 4.17: Blue shift of maximum absorbance of degraded RhB by MnO <sub>2</sub> nanoparticles synthesized by sol gel method under UV irradiation. ....	74

Figure 4.18: Removal efficiency (a) as a function of time and (b) at 12 min under UV irradiation (sol gel). .....	75
Figure 4.19: Photocatalytic mechanism of RhB removal by MnO <sub>2</sub> nanoparticles. ....	77
Figure 4.20: Effect of different scavengers on the removal efficiency of RhB dye using unwashed MnO <sub>2</sub> nanoparticles under UV irradiation after 12min. ....	78
Figure 4.21: Removal efficiency after repeatability test.....	79
Figure 4.22: FTIR spectrum of (a) RhB dye, unwashed MnO <sub>2</sub> nanoparticles synthesized by co-precipitation method (b) before and after dye removal without acid at (c) UV, (d) visible light and (e) dark condition, with addition of HCl at (f) UV, (g) visible light and (h) dark condition and with addition of H <sub>2</sub> SO <sub>4</sub> at (i) UV, (j) visible light and (k) dark condition. ....	80
Figure 4.23: Adsorption mechanism of RhB removal by MnO <sub>2</sub> nanoparticles.....	81
Figure 4.24: Oxidative degradation mechanism of RhB removal by MnO <sub>2</sub> nanoparticles. ....	83
Figure 4.25: XRD patterns of MnO <sub>2</sub> nanoparticles grown on wire coil at (a) 12W, (b) 18W, (c) 24W, (d) 30W and (e) 36W with growth time of 10min.....	85
Figure 4.26: Physical appearance of MnO <sub>2</sub> nanoparticles grown on wire coil at 12W, 18W, 24W, 30W and 36W for 10min. ....	85
Figure 4.27: SEM images of wire coil (a) before direct heating synthesis growth and after direct synthesis growth of MnO <sub>2</sub> nanoparticles for 10 minutes at (b) 12W and (c) 36W.. ....	86
Figure 4.28: SEM images of MnO <sub>2</sub> nanoparticles on wire coil synthesized at applied power of (a) 12W. (b) 18W, (c) 24W, (d) 30W and (e) 36W in growth solution for 10 minutes.....	88

Figure 4.29: XRD patterns of MnO <sub>2</sub> nanoparticles grown on wire coil at 24W with growth time of (a) 5min, (b) 15min, (c) 20min, (d) 25min and (e) 30min.	89
Figure 4.30: Physical appearance of MnO <sub>2</sub> nanoparticles grown on wire coil at 24W for 5min, 15min, 20min, 25min and 30min. ....	90
Figure 4.31: SEM images of MnO <sub>2</sub> nanoparticles on wire coil synthesized at an applied power 24W at growth solution for (a) 5min, (b) 15min, (c) 20min, (d) 25min and (e) 30min.. ....	91
Figure 4.32: Physical appearance of MnO <sub>2</sub> nanoparticles grown on wire coil at 12W, 18W, 24W, 30W and 36W for 10min after RhB dye removal test. ....	92
Figure 4.33: Removal efficiency of MnO <sub>2</sub> nanoparticles grown wire coil at different applied power for 10min under (a) UV, (b) visible light and (c) dark condition after 45min. ....	93
Figure 4.34: Physical appearance of MnO <sub>2</sub> nanoparticles grown on wire coil at 24W for 5min, 15min, 20min, 25min and 30min after RhB dye removal test. ....	94
Figure 4.35: Removal efficiency of MnO <sub>2</sub> nanoparticles grown wire coil at 24W with different growth time under (a) UV, (b) visible light and (c) dark condition after 45min.....	94

## **LIST OF ABBREVIATIONS**

AOP	Advanced Oxidation Process
EDX	Energy Dispersive X-ray
FESEM	Field Emission Scanning Electron Microscope
FTIR	Fourier transform infrared spectroscopy
HRTEM	High Resolution Transmission Electron Microscope
ICSD	Inorganic Crystal Structure Database
SEM	Scanning Electron Microscope
UV	Ultraviolet
XPS	X-ray Photoelectron Spectroscopy
XRD	X-Ray Diffraction

## LIST OF SYMBOLS

$^{\circ}\text{C}$	Degree celsius
$\text{\AA}$	Angstrom
$\text{H}_2\text{SO}_4$	Sulphuric acid
$\text{HCl}$	Hydrochloric acid
$\text{mg/L}$	Milligram per litre
$\text{min}$	Minute
$\text{MnO}_2$	Manganese dioxide
$\text{MnO}_x$	Manganese oxide
$\text{nm}$	nanometer
$\text{O}^{2-\bullet}$	Superoxide anion
$\text{OH}^{\bullet}$	Hydroxyl radical
$\text{RhB}$	Rhodamine B
$\text{TiO}_2$	Titanium oxide
$\text{W}$	Watt
$\text{ZnO}$	Zinc oxide
$\alpha\text{-MnO}_2$	Hollandite
$\beta\text{-MnO}_2$	Pyrolusite
$\gamma\text{-MnO}$	Ramsdellite

# **SINTESIS DAN PENCIRIAN NANOPARTIKAL MANGAN OKSIDA MELALUI CARA PEMANASAN LANGSUNG**

## **ABSTRAK**

Efluen berwarna dilepaskan daripada industri tekstil telah menjadi kebimbangan alam sekitar kritikal kerana ia susah terdegradasi. Proses pengoksidaan lanjutan (AOPs) menggunakan photocatalyst nampaknya merupakan rawatan efluen yang paling menjanjikan, tetapi kebanyakan photocatalyst mempunyai bandgap yang luas tidak praktikal dalam persekitaran sebenar kerana memerlukan sinaran ultraungu (UV) untuk diaktifkan. Masalah ditumbul apabila mengeluarkan photocatalyst daripada efluen yang telah dirawat selepas aplikasi. Dalam projek ini, kaedah pemendakan dan sol gel telah digunakan untuk menghasilkan nanopartikel  $\text{MnO}_2$  dan nanopartikel  $\text{MnO}_2$  juga ditumbuhkan di atas gegelung dawai Khantal melalui kaedah pemanasan langsung. Produk yang dihasilkan dicirikan dengan menggunakan pelbagai alat analisis seperti pembelauan sinar-X (XRD), spektroskopi fotoelektron sinar-X (XPS), mikroskop elektron pengimbas pancaran medan (SEM) dan mikroskop elektron penghantaran (TEM) dan digunakan untuk kajian penyingkiran pewarna di bawah UV, penyinaran cahaya dan keadaan gelap dengan penambahan asid hidroklorik (HCl) atau asid sulfurik ( $\text{H}_2\text{SO}_4$ ). Penyingkiran pewarna dengan menggunakan  $\text{MnO}_2$  nanopartikel sahaja adalah tidak berkesan. Tetapi, kecekapan penyingkiran mencapai 96.63% dan 57.93% selepas 12min untuk nanopartikel yang disintesis oleh kaedah pengangkatan dan sol gel masing-masing dengan penambahan  $\text{H}_2\text{SO}_4$ . Proses pencucian nanopartikel juga mempengaruhi kecekapan penyingkiran pewarna. Mekanisme nanopartikel untuk menyingkirkan pewarna adalah melalui degradasi oksidatif. Nanopartikel  $\text{MnO}_2$  yang mempunyai struktur hierarki telah ditumbuh di gegelung dawai dengan pelbagai kuasa pemanasan dan masa pertumbuhan. Proses nukleasi adalah jelas semasa peningkatan kuasa pemanasan



manakala pematangan Ostwald adalah jelas dengan peningkatan masa pertumbuhan. Nanopartikel  $\text{MnO}_2$  yang ditumbuhkan pada gegelung dawai boleh digunakan untuk proses penyingkiran dye. Nanopartikel  $\text{MnO}_2$  yang ditumbuhkan dengan kuasa pemanasan 30W dalam tempoh 10min dan tempoh pertumbuhan 30 minit pada 24W menunjukkan kecekapan tertinggi iaitu sebanyak 98.25% dan 85.69%.

# **SYNTHESIS AND CHARACTERIZATION OF MANGANESE DIOXIDE NANOPARTICLES VIA DIRECT HEATING METHOD**

## **ABSTRACT**

Coloured effluent discharged from textile industry has become critical environmental concern since it is difficult to be degraded. Advanced oxidation process (AOPs) using photocatalyst is one of the emerging techniques for effluent treatment, but most of the wide-bandgap photocatalyst is Ultraviolet (UV)-activated which is not practical in the real environment. Also, problem arises when there is a need to remove these photocatalyst in particle form from the treated effluent after application. In this project, narrow-bandgap  $\text{MnO}_2$  nanoparticles were synthesized using co-precipitation and sol gel methods.  $\text{MnO}_2$  nanoparticles were also grown on the Khantal wire coil via direct heating synthesis. The resulting products were characterised using various analytical tools (e.g. X-Ray Diffraction (XRD), X-Ray photoelectron spectroscopy (XPS), Scanning Electron Microscopy (SEM), Transmission Electron Microscope (TEM)) and were employed for dye removal study under UV, visible light irradiation and dark condition with addition of hydrochloric acid (HCl) or sulphuric acid ( $\text{H}_2\text{SO}_4$ ).  $\text{MnO}_2$  nanoparticles alone was not efficient in removing dye. With addition of  $\text{H}_2\text{SO}_4$ , removal efficiency reached 96.63% and 57.93% after 12min for nanoparticles synthesized by co-precipitation and sol gel methods respectively. Washing of nanoparticles with deionised water and ethanol influenced the dye removal efficiency. It was found that the removal mechanism of  $\text{MnO}_2$  nanoparticles was oxidative degradation

process. To minimise lost of nanoparticles, MnO<sub>2</sub> nanoparticles with hierarchical structures were grown on the wire coil with various heating power and growth time. Secondary nucleation was prominent with increasing heating power whereas Ostwald ripening was obvious with increasing growth time. Besides, MnO<sub>2</sub> nanoparticles grown on wire coil could be used for dye removal process. MnO<sub>2</sub> nanoparticles grown with heating power of 30W with 10min growth time and growth duration of 30min at 24W exhibited highest efficiency which were 98.25% and 85.69%, respectively.

# CHAPTER 1

## INTRODUCTION

### 1.1 Research background

Rapid development in industrialization and urbanization to meet the fast-growing population and living standard has caused water quality continues to deteriorate. Discharging of untreated effluent from various industries into water bodies has become the major cause of water pollution (Shahid and Butola, 2018). These wastewater discharge influences the composition and characteristic of a water body and its water quality level, leading to the water is unsuitable for human consumption (Organisation for Economic Co-operation and Development [OECD], 2017). Pollutants such as organic compounds, dyes and heavy metals must be removed to render the water potable or appropriate for other application. Based on the guidelines for drinking water quality from World Health Organization (WHO), the consumable water should not contain chemical that exceed maximum allowable concentration. For instance, the maximum tolerance value for colour in drinking water is 15 true colour units (TCU) (WHO, 2017).

In Malaysia, the water quality status is classified into three categories (clean, slightly polluted and polluted) that evaluated based on Water Quality Index (WQI) instead of exact values of river water quality measurements for individual monitoring sites. According to the analysis from Department of Environment (DOE), out of the 477 rivers monitored at year 2015 (Figure 1.1), 276 (58%) were identified to possess clean water quality index, 168 (35%) slightly polluted and 33 (7%) polluted. At the same year, a total of 2918478.34 metric tonnes of scheduled wastes were generated, whereby textile industries accounted 0.04% of total wastes produced which was 1040.38 metric tonnes (DOE, 2015). Despite textile industries contributed only 0.04% of total wastes produced,

more awareness regarding to the coloured effluent discharged is required as 22% of the total volume of industrial wastewater produced in Malaysia is actually owing to textile finishing wastewater (Pang and Abdullah, 2013).

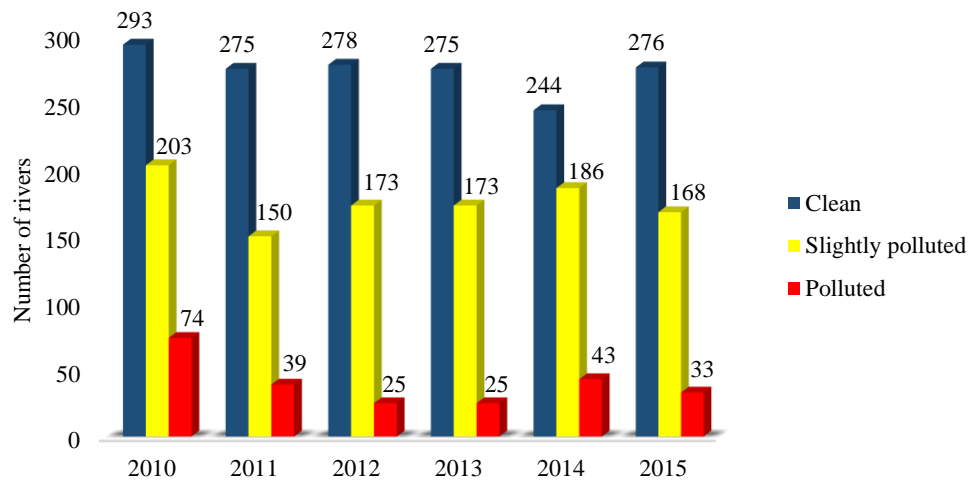


Figure 1.1: River water quality trend in Malaysia from year 2010 to year 2015 (DOE, 2015).

Large amount of water is used as chemicals dissolution medium and washing-off agent in textile processing. These water will be ended up with dye-rich and toxic wastewater and discharged to water bodies without appropriate treatment (Muthu, 2016). Among the chemicals in textile effluents, dyes are most harmful pollutant that rendering enormous environment threat. It is reported that there are more than 100,000 commercially available dyes in the textile industry. Owing to their high water solubility and relatively low molecular weight, they are readily to dissolve in water to form hardly biodegradable effluent (Parsons, 2004). Dye-containing effluent inhibits the sunlight from penetrating through the water and thus hindering the photosynthesis process of aquatic plants. Furthermore, dye molecules lower the water quality and are carcinogenic to human (Shahid and Butola, 2018). The major sources of textile industry wastewater pollution were mostly located in East Coast of Peninsular Malaysia as shown in Figure

1.2. It is recorded that the majority of potentially polluted sources of textile industry located at Johor, Pulau Pinang and Selangor.

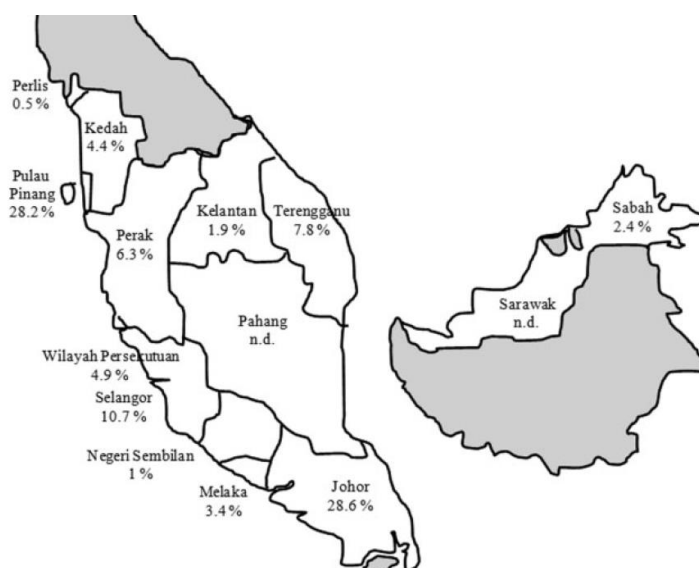


Figure 1.2: Distribution of wastewater release from textile industry in Malaysia (Pang and Abdullah, 2013).

Recent research attention has emphasized on the remediation of colour from textile effluent as most of the wastewater treatment in textile industry are incapable to remove the dye to satisfactory levels. Conventional treatments such as membrane filtration, coagulation and flocculation, biological treatment and ion exchange have their own limitation in removing dye molecules (Wang et al., 2009). Moreover, certain form of colour is difficult to be removed by a single conventional treatment due to the high stability of modern dyes (Mishra, S. B. and Mishra, A. K., 2017). Advanced oxidation processes (AOPs) has been at the forefront of research attention in the recent days since it is capable to treat dye molecules in the textile effluents effectively. AOPs have the ability to oxidize non-biodegradable compounds with the aid of highly reactive radicals (Mohabansi et al., 2011). Heterogeneous catalysis using semiconductor particles employed by AOPs is a promising technology for the reduction of global environmental

pollution (Mittal et al., 2009). Particularly, titanium dioxide (TiO<sub>2</sub>) and zinc oxide (ZnO) have gained immense research interest due to their effectiveness in removing organic dyes under ultraviolet (UV) spectrum (Mondal and Sharma, 2014).

Owing to the wide bandgap of TiO<sub>2</sub> (3.2eV) and ZnO (3.3eV), these photocatalysts can only be activated under the UV light irradiation which restrict their use only to outdoor applications. TiO<sub>2</sub> and ZnO are normally doped with transition metals like ferum (Fe), nickel (Ni), copper (Cu), chromium (Cr) and magnesium (Mg) ions to substitute host ions with dopant ions in the lattices which can narrow their bandgap and increase the electrons delocalization in the nanostructure, subsequently enhancing their photocatalytic performance (Li et al., 2017). In addition, coupling of composite semiconductors is also commonly practiced to shift the optical sensitivity of TiO<sub>2</sub> and ZnO from UV to the visible region (Xin et al., 2012). As a result, it is highly desired to seek for visible-light-driven photocatalyst as an alternative to TiO<sub>2</sub> and ZnO. Amongst the metal oxide semiconductors, manganese dioxide (MnO<sub>2</sub>) is a suitable candidate due to its nontoxicity, low cost, easy obtainment and most importantly its narrow bandgap (1.3eV) which allow it to be activated by visible light and theoretically even infrared light (Nevárez-Martínez et al., 2017; Qin et al., 2017).

There are several routes have been reported for the synthesis of MnO<sub>2</sub> with various shapes and excellent properties, such as hydrothermal method (Miao et al., 2015; Yuan et al., 2014; Qiu et al., 2011), sol-gel synthesis (Ivanets et al., 2018; Tang et al., 2014), green methods (Sanchez-Botero et al., 2017; Kumar et al., 2017; Moon et al., 2015) and co-precipitation (Kanhua and Saengkwamsawanga, 2017; Cherian et al., 2016; Ramprasath et al., 2016; Kumari et al., 2015). However, most of the MnO<sub>2</sub> nanostructures synthesized by these approaches are in the form of powders, resulting the need of

removing MnO<sub>2</sub> after introducing it in wastewater application. With that, there is a need to endow an alternative synthesis method that can minimise the problem mentioned.

## **1.2 Problem statement**

Various photocatalysts have been introduced in treating effluent, but most of them are wide bandgap metal oxides which exhibit poor removal efficiency under visible light. MnO<sub>2</sub> is narrow bandgap metal oxide which can serve as an alternative to the photocatalyst used in water treatment. To date, several MnO<sub>2</sub> synthesis methods have been employed by researchers to explore its application in various field. Most of the photocatalytic reduction and decomposition involve the use of nanoscale semiconductor in the form of colloidal suspension. This incurs the need of extra cost and time in removing the particles from the system (Ibhadon and Fitzpatrick, 2013). Besides, nanoscale materials have higher tendency to become agglomerated while dispersed in an aqueous medium which decreases their photocatalytic efficiency. Chan et al. (2016) and Aziz et al. (2017) reported the growth of  $\beta$ -MnO<sub>2</sub> nanotubes on polyethylene terephthalate (PET) fibre and growth of tungsten oxide (WO<sub>x</sub>) layer on PET fiber respectively to rectify the problems mentioned. However, a seed layer is usually required to be deposited on the polymer fiber prior to the growth of metal oxide to enhance the adhesion between the polymer fiber and metal oxide. The deposition of seed layer is often accompanied by drawbacks such as the need to prepare seed solution. It is known that properties and applications of nanomaterials greatly depend on their phases, sizes and morphologies (Liu et al., 2013). Therefore, it is necessary to introduce a new method to synthesize and to grow MnO<sub>2</sub> nanostructure on the substrate without deposition of seed layer. No other work is found to report on the formation of MnO<sub>2</sub> nanstructures via direct heating method.



### 1.3 Research objectives

The main objectives of this research are:

1. To synthesize and characterize MnO<sub>2</sub> nanoparticles using co-precipitation and sol gel methods
2. To synthesize and characterize MnO<sub>2</sub> nanoparticles on wire coil using direct heating method
3. To access Rhodamine B (RhB) dye removal properties of MnO<sub>2</sub> nanoparticles under acid condition (e.g. HCl, H<sub>2</sub>SO<sub>4</sub>)

### 1.4 Project overview

In this project, the synthesis processes were divided into two parts; the first part was to synthesize MnO<sub>2</sub> nanoparticles in the form of powder through co-precipitation and sol gel methods, the second part was to grow MnO<sub>2</sub> nanoparticles on the wire coil with precursors employed in co-precipitation method via direct heating method. The electrical power applied and growth time were varied during direct heating synthesis to investigate the effect of heating power and growth time on the nanoparticles formed on the Khantal (Fe, Al, Cr) wire coil. MnO<sub>2</sub> nanoparticles in the form of powder were characterized using X-Ray Diffraction (XRD), X-Ray photoelectron spectroscopy (XPS), Field Emission Scanning Electron Microscopy (FESEM), Transmission Electron Microscope (TEM), Fourier-transform infrared spectroscopy (FTIR) and Zetasizer. Meanwhile, the phase presence and surface morphology of MnO<sub>2</sub> nanoparticles grown on wire coils were characterized using XRD and SEM respectively.

A series of RhB removal test was performed using MnO<sub>2</sub> nanoparticles (powder form) with and without addition of acid (e.g. HCl, H<sub>2</sub>SO<sub>4</sub>) under UV, visible and dark conditions to determine the RhB dye removal efficiency of MnO<sub>2</sub> nanoparticles under

different set of conditions.  $\text{MnO}_2$  nanoparticles were then filtered, dried at desiccator and characterized using FTIR after RhB dye removal test. After that, scavenger test with various reagents species was carried out with  $\text{MnO}_2$  nanoparticles to identify the main species involved during RhB dye removal process. Another series of RhB dye removal test was conducted using  $\text{MnO}_2$  nanoparticles grown wire coils under the condition that  $\text{MnO}_2$  nanoparticles showed high removal efficiency which has predetermined during RhB dye removal study using  $\text{MnO}_2$  nanoparticles (powder form).

### **1.5 Thesis outline**

This thesis comprises of five chapters. Chapter 1 includes the research background, problem statement, research objectives and project overview. Chapter 2 focuses on the conventional methods employed in wastewater treatment and manganese oxide ( $\text{MnO}_x$ ) synthesis methods reported in literature. Experimental details and characterization methods are described in Chapter 3. The experimental details cover the synthesis of  $\text{MnO}_2$  nanoparticles by co-precipitation, sol gel and direct heating methods and RhB dye removal study. In Chapter 4, experimental results of the research, data analysis and findings in relation to the theoretical body of knowledge are addressed. Lastly, conclusion and recommendations for future work are depicted in Chapter 5.

## CHAPTER 2

### LITERATURE REVIEW

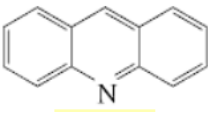
#### 2.1 Introduction

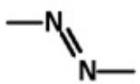
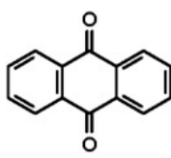
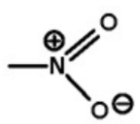
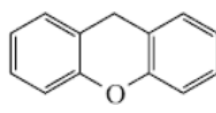
In recent times, colour removal from effluent has been a matter of concern since colour is the first issue to be recognised in effluent. The first part of this chapter highlights the root cause of coloured effluent and the removal of colour contaminant through conventional methods. In addition, the crystallographic data and properties of some  $\text{MnO}_2$  polymorphs are depicted. The later part of this chapter describes the  $\text{MnO}_x$  synthesis via various synthesis approaches that has been reported in literature and lists out the applications of  $\text{MnO}_x$ .

#### 2.2 Dyes and their classification

Dyes are coloured organic compound that responsible for imparting permanent colour by selective absorption of visible light (400-700nm) to a substrate such as cloth, paper, plastic or leather (Sharma, 2015). The two basic components of dye molecules are chromophore and auxochrome. The chromophores are important for colour production whereas auxochromes render the water-soluble properties of dye molecules and provide enhanced affinity toward fiber (Hung et al., 2012). Amongst the most important dyes, the classification based on chemical structure (type of chromophores) is depicted in Table 2.1.

Table 2.1: Classification of dyes based on chemical structure (Gaya, 2013; Madan, 2013).

Classes	Chromophoric structure	Description	Example
Acridine		Contain acridine nucleus	Acriflavin, Proflavin

Azo		Contain at least one azo groups (-N=N-) which form bridges between two or more aromatic rings	Congo red, Methyl orange
Anthraquinone		Contain one or more carbonyl group in association with a conjugated system	Disperse Red 60, Disperse Blue 60
Nitro		Contain at least one nitro group (-NO <sub>2</sub> -) in ortho- or para-position attached to the hydroxyl group	Napthol
Xanthene		Contain xanthylium or xanthene nucleus	RhB

### 2.3 Major sources of organic dye pollutants and their effects to human and environment

Organic dyes consist of complex aromatic molecular structures, making them more stable and harder to be degraded. Most of the dyes are reluctant to fade on exposure to light, water and chemicals because of their stable chemical structure (Abid et al., 2012). As a result, coloured wastewater remains one of the main environmental issues.

Industries activities generate huge amount of chemical wastes which causes water pollution. Amongst the industries, textile industry produces large quantities of coloured effluent due to large consumption of water in textile processing, dyeing and printing (Malik and Grohmann, 2012). In fact, about 1.6 million liters of water was consumed in average-sized textile mill with production of about 8000 kg of fabric per day (Kant, 2012). In Malaysia, textiles and textile products industries were tenth largest export earner, contributing approximately 2.1% to total exports of manufactured goods (Malaysian Investment Development Authority, 2016). Textile industry is growing

steadily as a result of escalating export demand of textile and clothing products (Figure 2.1) which substantially contributes to the economic growth in Malaysia.

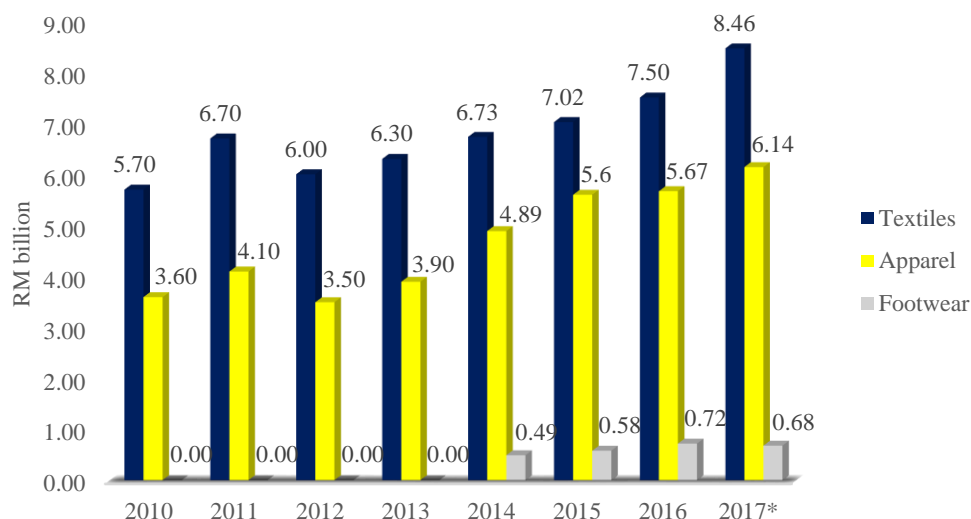


Figure 2.1: Export demand of textiles and textile products in Malaysia from 2010 to 2017 (in billion) (Ministry of International Trade and Industry [MITI], 2017).

Enormous emphasis is now given to serve the niche market and upstream activities demands, it is expected that textiles industry will continue to liberalise and widen in future years. However, the growth of textile industry is in fact at the expense of the environmental quality especially with respect to the liquid effluent (Pang and Abdullah, 2013). Besides textile industry, other industries such as paper and pulp mills, dyestuff, distilleries, and tanneries are also generating highly coloured effluents.

Releasing of coloured effluents in the ecosystem results adverse effects to both human and environment. The transparency and quality of water bodies are detrimental with the presence of very small amounts of dyes (<1 mg/L for some dyes) in water (Chequer et al., 2013). Industrial effluents that contain organic dyes reduce light penetration, hampering aquatic lives and hindering photosynthesis. This in turn affects the food source of aquatic organisms. It is noteworthy that dyes are difficult to be

degraded, causing them remain in the environment for a long period of time. Owing to the presence of carcinogens such as naphthalene, benzamine and other aromatic compound, discharged dyes and their breakdown products are normally toxic, carcinogenic and mutagenic to health (Saini, 2017). Besides, dyes can also cause skin irritation, irritation to mucous membrane and respiratory problems due to the contact or inhalation of dye particles (Hassaan and Nemr, 2017).

Amongst the various organic dyes, emphasis would be placed on RhB dye in this project as it is one of the widely used xanthene dyes in textiles and food stuffs and has become a common organic pollutant.

## **2.4 Conventional methods of organic dye removal**

Textile dye wastewater remediation is based not only in decolourisation, but also in the degradation and mineralization of the dye molecules. Different separation techniques have been employed in the removal of dyes from textile effluents.

### **2.4.1 Adsorption**

Adsorption technology is an equilibrium separation process which is effective and economical in removing organic dye from waste stream. Adsorption is a surface phenomenon that substance is accumulated at the interface between two phases. This process involves the transfer and adhesion of the ions, atoms or molecules of the adsorbate to its surface, leading to thin film formation (Deaconu et al., 2016). Adsorbate refers to the substance that retains at the interface whereas adsorbent indicates the solid on which adsorption occurs. Adsorbents are in general highly porous and have a large surface area. The interaction and the adsorption capacity of adsorbents are greatly relied on zeta potential (Yagub et al., 2014). Adsorption technique is divided into physical adsorption (physisorption) and chemical adsorption (chemisorption). Physical adsorption happens

reversibly by weak interactions such as Van der Waals interactions, hydrophobicity, polarity, hydrogen bonding and dipole-dipole interaction. On the other hand, chemical adsorption occurs irreversibly via strong interactions that normally involve exchange of electrons, such as covalent and ionic bonding between adsorbate and adsorbent (Sharma, 2015). Examples of dye adsorbents are activated carbon, silicon dioxide ( $\text{SiO}_2$ ), alumina ( $\text{Al}_2\text{O}_3$ ), calcium oxide ( $\text{CaO}$ ), magnesium oxide ( $\text{MgO}$ ), iron (III) oxide ( $\text{Fe}_2\text{O}_3$ ), sodium oxide ( $\text{Na}_2\text{O}$ ), potassium oxide ( $\text{K}_2\text{O}$ ), bentonite, and montmorillonite (Julkapli et al., 2014).

#### **2.4.2 Membrane filtration**

Membrane technology encompasses the implement of different filtration techniques, which separate the dissolved, colloidal and particulate constituents from a pressurized fluid. Membrane filtration techniques can be distinguished based on pore size of membrane. Generally, they are classified as microfiltration ( $0.02\text{-}10\mu\text{m}$ ), ultrafiltration ( $0.001\text{-}0.02\mu\text{m}$ ), nanofiltration ( $0.001\text{-}0.002\mu\text{m}$ ) and reverse osmosis ( $0.0001\text{-}0.001\mu\text{m}$ ) (Sinha and Parameswar, 2012). Microfiltration and ultrafiltration membranes have larger pores and they allow the removal of colloidal substances and microorganisms. Owing to the smaller pore sizes of nanofiltration and reverse osmosis membranes and higher operating pressure, nanofiltration and reverse osmosis capable to separate dissolved substances such as micropollutants and ions from the stream besides removing colloidal substances and microorganisms (Sogaard, 2014). Membrane acts as a semipermeable barrier that allows selective components to permeate while retaining the passage of other components during filtration process as shown in Figure 2.2, resulting complete separation of two components. The transport of the permeable components through the membrane is driven by pressure (Mohanty and Purkait, 2011).

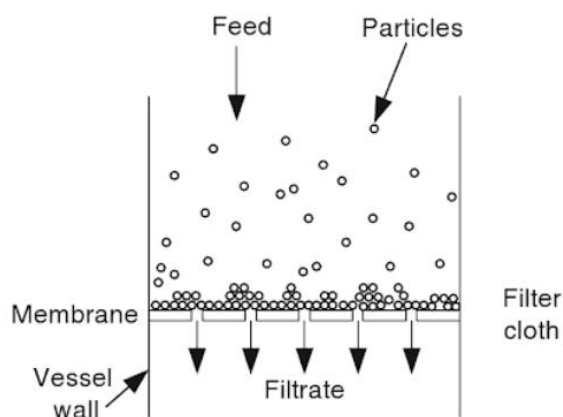


Figure 2.2: Principle of surface filtration using membrane or filter cloth (Sirkar, 2014).

### 2.4.3 Ion exchange

Both cationic and anionic dyes can be eliminated from effluents using ion exchange method by passing the coloured wastewater through the beds of ion exchanger (Figure 2.3). Ion exchange is a reversible chemical process wherein there is an exchange of ion from effluent with similarly charged ion attached to immobile ion-exchange solid particle. These exchanges occurs without any physical alteration to the ion exchanger (Mishra and Clark, 2013). There are plenty of ion exchangers available, whether natural or synthetic. Fixed ionic groups exist in all ion exchangers, which are balanced by counter ions of opposite charge within the matrix to maintain electroneutrality (Dege, 2011). Counter ions can permeate in and out of the molecular framework of the solid matrix and may be exchanged stoichiometrically with other dissolved ions of the same charge from external solution. Exchange will be ceased when equilibrium is reached, in which the available exchange sites are saturated (Grandison, 1996).



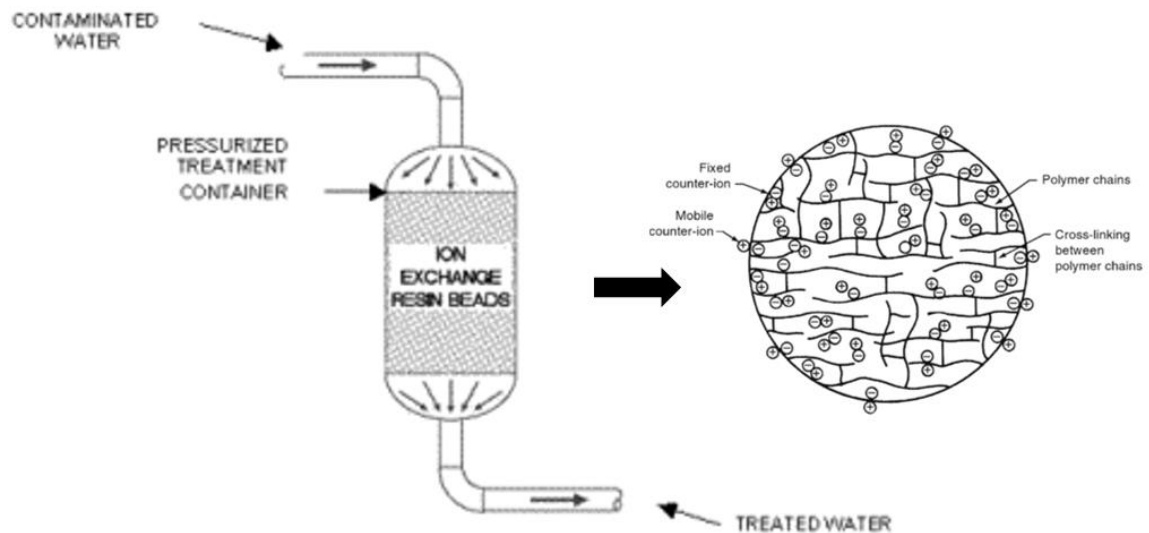


Figure 2.3: Schematic diagram of ion exchange process with generalised cation-exchanger bead which bearing fixed negative charges (Dege, 2011).

#### 2.4.4 Coagulation-flocculation

Coagulation-flocculation is a physicochemical method employed for colour removal in wastewater treatment. Coagulation-flocculation in wastewater treatment process can be divided into two distinct procedures which are coagulation and flocculation (Tzoupanos and Zouboulis, 2008). Coagulation involves particles destabilization of colloidal suspension by repulsive forces reduction which achieved by adding of coagulant agents. Coagulants have charges that are opposite to suspended solids and they are used to neutralize the negative charges on dispersed non-settable solids. Examples of coagulants used in wastewater treatment are aluminum sulfate or alum ( $\text{Al}_2(\text{SO}_4)_3 \cdot 18\text{H}_2\text{O}$ ), lime ( $\text{Ca}(\text{OH})_2$ ) and ferric salt such as ferric sulfate ( $\text{Fe}_2(\text{SO}_4)_3 \cdot 7\text{H}_2\text{O}$ ) or ferric chloride ( $\text{FeCl}_3 \cdot 7\text{H}_2\text{O}$ ) (Pang et al., 2013). Coagulation is followed by flocculation which is induction process of destabilized particles to allow them make contact and form large agglomerates, which can be separated easier by sedimentation (Wang et al., 2007). The overall coagulation-flocculation process is illustrated in Figure 2.4.

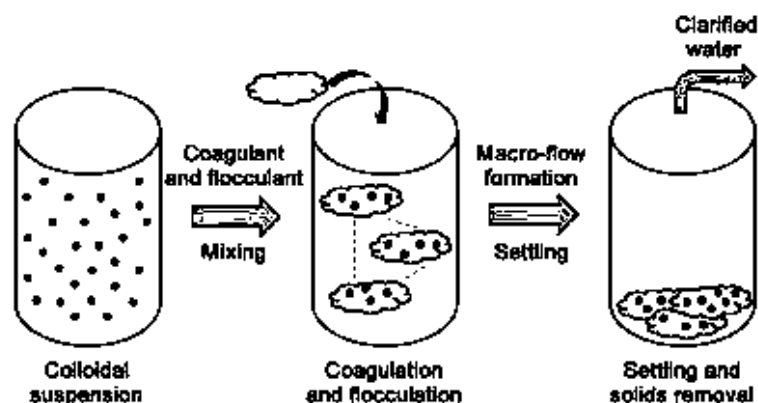


Figure 2.4: Coagulation and flocculation processed of a colloidal suspension (Wang et al., 2007).

#### 2.4.5 Aerobic / anaerobic degradation

Both aerobic and anaerobic degradation are biological wastewater treatment used to degrade dye compounds. They can be used together or separately in treating coloured effluents. Aerobic degradation takes place in the oxygen-rich environment with microorganism called aerobes. In this case, aerobes utilise oxygen to assimilate organic impurities which are then converted into carbon dioxide, water and biomass. On the other hand, anaerobic degradation occurs in the absence of oxygen with microorganisms called anaerobes. Anaerobes capable to convert organic substances into methane, carbon dioxide and biomass in environment with no oxygen (Sharma, 2015).

#### 2.4.6 AOPs

AOPs decolourise dye containing effluent by generating highly reactive species like hydroxyl radical ( $\text{OH}\cdot$ ) with strong oxidative potential ( $E_o = +2.8\text{V}$ ). These radicals capable to oxidise a broad range of organic pollutants in a non-selective manner (Bhatia, 2017). Basically, there are two stages of oxidation involved in AOPs which are the formation of strong oxidants and the reaction of these oxidants with organic pollutant in effluent. Various AOPs are available to generate  $\text{OH}\cdot$ , including Fenton's reaction,

ozonation, sonocatalytic degradation, semiconductor catalysis and electron beam irradiation. All of these processes have different mechanisms for destroying organic pollutants, in which their removal effectiveness is proportional to its ability to produce OH• (Cheng et al., 2012). The summarised reactions of various AOPs in producing OH• are depicted in Table 2.2.

Table 2.2: Common AOPs and reactions involved in each process (Krishnan et al., 2017; Deng and Zhao, 2015).

Processes	Reactions involved
Fenton's reaction	<i>Generation of hydroxyl radical</i> $\text{Fe}^{2+} + \text{H}_2\text{O}_2 \rightarrow \text{Fe}^{3+} + \text{OH}^- + \text{HO}\bullet$ <i>Regeneration of <math>\text{Fe}^{2+}</math> ions</i> $\text{Fe}^{3+} + \text{H}_2\text{O}_2 \rightarrow \text{Fe}^{2+} + \text{HO}_2\bullet + \text{H}^+$
Ozonation	<i>Formation of hydroxyl radical using water</i> $3\text{O}_3 + \text{OH}^- + \text{H}^+ \rightarrow 2\text{HO}\bullet + 4\text{O}_2$ <i>Formation of hydroxyl radical using hydrogen peroxide (<math>\text{H}_2\text{O}_2</math>)</i> $2\text{O}_3 + \text{H}_2\text{O}_2 \rightarrow 2\text{HO}\bullet + 3\text{O}_2$
Sonocatalytic degradation	<i>Generation of hydroxyl radicals through fragmentation of water molecules in the form of gas within microbubbles</i> $\text{H}_2\text{O} \rightarrow \text{OH}\bullet + \text{H}\bullet$
Photocatalysis (eg: $\text{TiO}_2$ )	<i>Generation of electrons and holes</i> $\text{TiO}_2 + h\nu \rightarrow \text{e}^- + \text{h}^+$ <i>Formation of superoxide radical anions (<math>\text{O}_2^{\bullet-}</math>)</i> $\text{e}^- + \text{O}_2 (\text{absorbed}) \rightarrow \text{O}_2^{\bullet-}$ <i>Interaction of hole with water</i> $\text{h}^+ + \text{H}_2\text{O} (\text{absorbed}) \rightarrow \text{H}^+ + \text{HO}\bullet$
Electron beam irradiation	<i>Generation of various free radicals through water splitting</i> $\text{H}_2\text{O} + \text{e}^- \rightarrow 2.7 \text{OH}\bullet + 2.7 \text{H}_3\text{O}^+ + 2.6 \text{e}^- + 0.7 \text{H}_2\text{O}_2 + 0.6 \text{H}\bullet + 0.45 \text{H}_2$

#### 2.4.6.1 Photocatalysis technique using semiconductor materials

Since semiconductor-based photocatalysis is the main interest of this project, it is further discussed in this sub-section. Photocatalytic reaction is initiated when light with energy equal to or higher than the bandgap energy of semiconductor photocatalyst is

irradiated on the surface of semiconductor photocatalyst, electron-hole pairs are formed by promoting photoelectron from the filled valence band to the empty conduction band. It is then followed by ionization of water, whereby photogenerated holes at the valence band react with water to produce  $\text{OH}^\bullet$  radical. These radical possess powerful oxidizing power which capable to attack adsorbed organic molecules or those are in close proximity to the photocatalyst surface non-selectively, converting them into less harmful end products like carbon dioxide and water. At the same time, electron in the conduction band is consumed by the oxygen to generate anionic  $\text{O}_2^{\bullet-}$ .  $\text{O}_2^{\bullet-}$  is then protonated ( $\text{H}^+$  in water), forming hydroperoxyl radical ( $\text{HO}_2^\bullet$ ) and subsequently converted to  $\text{H}_2\text{O}_2$  which further dissociates into highly reactive  $\text{OH}^\bullet$ . (Ajmal et al., 2014). The schematic representation of photocatalytic degradation mechanism for RhB dye is illustrated in Figure 2.5.

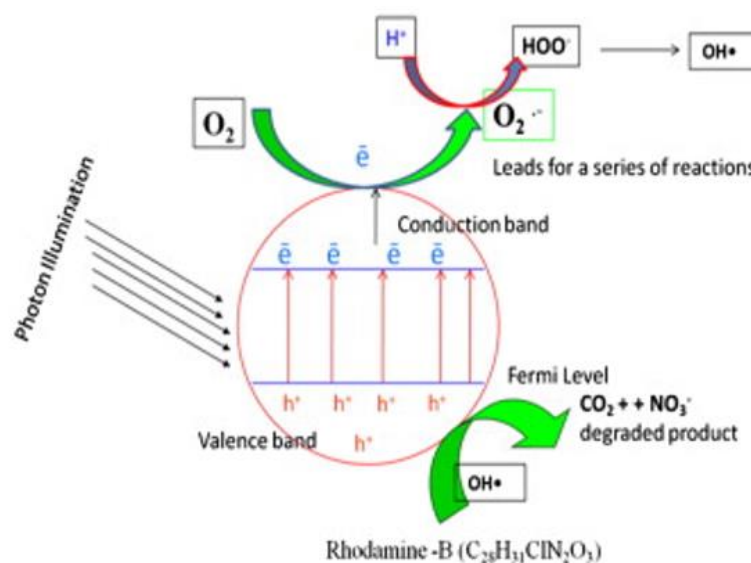


Figure 2.5: Schematic diagram of RhB degradation mechanism (Rahman et al., 2013).

Number of semiconductors have been extensively studied to use as photocatalysts for the removal of different organic dyes from effluent, including metal oxides (e.g.  $\text{TiO}_2$ ,  $\text{ZnO}$ ,  $\text{Fe}_2\text{O}_3$ ,  $\text{CuO}$ ), perovskite-type oxide (e.g. strontium titanate ( $\text{SrTiO}_3$ )) and sulphides (e.g. cadmium sulphide ( $\text{CdS}$ ), zinc sulphide ( $\text{ZnS}$ )). Excitation

by visible light is possible for binary metal sulphides and selenide semiconductors, such as CdS, lead (II) sulphide (PbS) and cadmium selenide (CdSe), owing to their narrower bandgaps than metal oxides. Nevertheless, these materials are toxic and insufficiently stable for photocatalysis since they encounter photoanodic corrosion in aqueous media under UV irradiation. In the case of p-type semiconductors, they are rarely employed in photocatalysis as their bandgap energies are too small and most of these materials are unstable. As a result, immense interest is paid on wide bandgap n-type semiconductors like  $\text{TiO}_2$ ,  $\text{WO}_3$ ,  $\text{SrTiO}_3$  and  $\text{ZnO}$ . These materials are effective photocatalysts because they render sufficiently high reduction and oxidation potentials in their conduction band and valance band respectively (Triantafyllidis et al., 2013). Amongst the metal oxide semiconductors,  $\text{TiO}_2$  and  $\text{ZnO}$  are nominated to be promising photocatalyst in effluent treatment. The major drawback of these materials is the need of high energy input, only near UV light is able to be absorbed for activation. UV light has low penetration ability in water medium and hence these photocatalysts are restricted to lightly colored effluent that has low dye concentration (Pang et al., 2013). With that, there is a requirement to search for alternative metal oxide photocatalysts that work well under light from the visible spectral region.

The principal advantages and disadvantages of different dye removal methods as discussed in section 2.4 are listed in Table 2.3.

Table 2.3: Advantages and disadvantages of different dye removal methods.

Process	Advantages	Disadvantages
Adsorption (Xing et al., 2016)	✓ Use of low-cost materials, simple and sludge-free	✗ Effectiveness depends on the characteristics of the absorbent ✗ Low adsorption capacity
Ion exchange (Sharma, 2015)	✓ No absorbent loss on regeneration	✗ Wide range of dyes is not able to accommodate ✗ Not effective for disperse dye ✗ High cost of organic solvents to regenerate the ion exchanger
Coagulation-flocculation (Muthu, 2015; Mane and Babu, 2011)	✓ Decolourization of dye effluent is done by removal of dye molecules instead of partial decomposition of dye ✓ Capable to eliminate insoluble dyes	✗ Formation of large quantities of chemical sludge ✗ High cost for sludge disposal
Membrane filtration (de Voogt, 2015; Mishra and Clark, 2013)	✓ Quick and low spatial requirement ✓ Remove all type of dye effectively ✓ Recover and recycle chemicals (dyes) while producing reusable water	✗ High membranes cost and working pressures ✗ Clogging and fouling of the membrane by dyes after long usage ✗ Low lifespan of membrane
Aerobic / anaerobic degradation (Chen et al., 2011; Rai et al., 2007)	✓ Mineralization of the dyes to harmless inorganic compounds ✓ Formation of a lesser quantity of relatively harmless sludge ✓ Does not required harmful chemical other than nutrients	✗ Relatively slow degradation rate ✗ Most of the synthetic dyes are resistant to degradation by bacteria ✗ Not effective if the concentration of organic pollutants is very high

<p>AOPs using semiconductor materials (Krishnan et al., 2017; Feitz, 2005)</p>	<ul style="list-style-type: none"> <li>✓ Environmental-friendly, low consumption of energy, relatively inexpensive, having high surface area</li> <li>✓ Regeneration and reuse of photocatalysts are possible</li> <li>✓ Exhibit tunable properties which can be modified by size reduction and doping</li> <li>✓ Fast reaction rates and non-selective oxidation, allowing the simultaneous removal of multiple pollutants</li> <li>✓ Solar energy can be employed for systems that do not require fast throughput</li> <li>✓ Transformation of organic compounds to simpler compounds or to carbon dioxide and water with no sludge production</li> </ul>	<ul style="list-style-type: none"> <li>✗ Require optimum conditions for high effectiveness</li> <li>✗ Difficult in catalyst separation and immobilization</li> <li>✗ Deterioration of lamp performance at high temperatures</li> <li>✗ Colour reduces efficiency since light cannot penetrate through</li> </ul>
--	---	--

#### 2.4.6.2 Remediation of dye using MnO<sub>x</sub>

Numerous studies have reported the organic dye removal by various photocatalysts like TiO<sub>2</sub> and ZnO. Despite these wide bandgap semiconductors show promising results, the photosensitivity of these semiconductors are limited to the wavelengths below 400nm (UV region), which consists merely 3% of the overall solar energy spectrum. Therefore, direct use of solar energy for photocatalytic degradation of organic dye using these photocatalysts is less practical. As a result, attention has been shifted in searching for visible-light-driven photocatalysts for organic compounds removal as solar spectrum comprises of about 44% of visible light.

In this regard, MnO<sub>2</sub> and its composite are suitable candidates for organic dye removal. Several researchers found that the removal of dye by various MnO<sub>2</sub> is actually through photocatalytic degradation and adsorption. Crystallographic forms of MnO<sub>2</sub> which may be layered or tunnel structures formed by different arrangements of MnO<sub>6</sub> octahedral influence the removal efficiencies of the dye pollutants. Cui et al. (2015) reported that MnO<sub>2</sub> with different crystal type exhibit different dye removal efficiency at different pH. Considerable research efforts have been devoted to synthesize MnO<sub>2</sub> and their composite with improved dye removal efficiency. For instance, Gong et al (2017) have developed MnO<sub>2</sub>-SiO<sub>2</sub> nanocomposite which exhibited much higher efficiency for degradation of RhB than MnO<sub>2</sub>; Dang et al. (2016) prepared composite of amorphous MnO<sub>2</sub> and diatomaceous earth (so called diatomite or bio-silica) to catalytically degrade methylene blue and methyl orange at ambient conditions; Hao et al. (2013) synthesized urchin-like Mn<sub>3</sub>O<sub>4</sub>/MnO<sub>2</sub> hollow nanostructures mixture to degrade RhB in acid condition without light stimulation and addition of H<sub>2</sub>O<sub>2</sub> and Chen et al. (2011) compared performance of non-calcined porous magnetic MnO<sub>2</sub> and calcined porous magnetic MnO<sub>2</sub> in removing methylene blue. Besides, Sun et al. (2017) have fabricated MnO<sub>2</sub> aerogels and they have proved that MnO<sub>2</sub> aerogels with larger surface area and better crystalline possess



enhanced oxidative degradation efficiency compared to those of the commercial  $\text{MnO}_2$  powder and  $\text{MnO}_2$  nanosheets due to easier passage of RhB and its degradation products during the reaction in  $\text{MnO}_2$  aerogels. Table 2.4 summarises several reports on the removal of different organic dye using  $\text{MnO}_2$ .

## 2.5 Manganese (Mn) and $\text{MnO}_x$

Mn is a transition metal and exhibits a number of oxidation states. The three most common states are Mn(II), Mn(III) and Mn(IV). In this regard,  $\text{MnO}_x$  can exist in variety of stoichiometries, phases (e.g. manganese (II) oxide ( $\text{MnO}$ ),  $\text{MnO}_2$ , manganese (III) oxide ( $\text{Mn}_2\text{O}_3$ ) and manganese (II,III) oxide ( $\text{Mn}_3\text{O}_4$ )) and morphologies (Sharrouf et al., 2015). This section will be limited to those that are relevant for  $\text{MnO}_2$ .  $\text{MnO}_2$  has over 14 polymorphs with hexagonal, tunnel, layered, and spinel structures. Internal tunnel structures with sizes that commensurate with that of cations can act as host lattices for the insertion and extraction of cations (Luo, 2007). The existence of difference crystal structures is owing to the different corner and/or edge sharing arrangements of the unit building block, i.e.,  $\text{MnO}_6$  octahedron to form one-dimensional channels, resulting to the different thermal and electrochemical properties of  $\text{MnO}_2$  (Moon et al., 2012). Crystallographic data and properties of some  $\text{MnO}_2$  polymorphs are summarised as Table 2.5. The  $\text{MnO}_2$  polymorphs with well-defined crystalline phases are shown in Figure 2.6.

Table 2.4: Summary of utilisation of manganese oxide on different dye removal.

Photocatalyst	Microstructure	Type of dye	Dye concentration (mg/L)	Loading (mg)	pH	Light source	Removal percent (%)	Removal time (min)	Reference
MnO <sub>2</sub> -SiO <sub>2</sub> nanocomposite	Nanorod	RhB dye	500	500	2.5	Visible light	84.9	90	(Gong et al., 2017)
MnO <sub>2</sub> aerogels	3D percolating network with open pores	RhB dye	5	50	2.5	Dark room	97.6	10	(Sun et al., 2017)
Amorphous MnO <sub>2</sub> coated diatomite nanocomposite	Worm-like fibers structure formed by nanospheres	Methylene blue	20	250	5	Visible light	~75	30	(Dang et al., 2016)
		Methyl orange	33	250			~75		
$\alpha$ -MnO <sub>2</sub>	Needle-like nanostructures	RhB dye	10	500	2	Visible light	>90	5	(Cui et al., 2015)
					3		>90	10	
					4		~80	120	
					6		~80	120	
$\beta$ -MnO <sub>2</sub>	Rod-like shape				2		~80	120	
					3		50	120	
					4		<20	120	
					6		0	120	
$\delta$ -MnO <sub>2</sub>	3D hierarchical				2		>90	5	

	microsphere				3		80	120	
					4		<20	120	
					6		0	120	
Mn <sub>3</sub> O <sub>4</sub> /MnO <sub>2</sub>	Urchin-like hollow nanostructures	RhB dye	10	100	3	Dark room	90-97	60	(Hao et al., 2013)
Porous magnetic MnO <sub>x</sub>	Spherical nanoparticles	Methylene blue	100	200	7.6	Visible light	44.2	60	(Chen et al., 2011)
Porous magnetic MnO <sub>x</sub> (calcined)							~90	60	